Roles of phase separation and crystallization in the structure formation of new segmented polyurethane ureas and their nanocomposites with single-walled carbon nanotubes*

M. A. Gorbunova,[a,b] D. V. Anokhin,[a,b,c]★ V. Yu. Zaitsev,[b] A. A. Grishchuk,[a] and E. R. Badamshina[a]

[a] *Institute of Problems of Chemical Physics, Russian Academy of Sciences, 1 prosp. Akad. Semenova, 142432 Chernogolovka, Moscow Region, Russian Federation. E-mail: deniano@yahoo.com*
[b] *M. V. Lomonosov Moscow State University, 1-51 Leninskie Gory, 119991 Moscow, Russian Federation*
[c] *Moscow Institute of Physics and Technology (National Research University), 9 Institutskiy per., 141701 Dolgoprudny, Moscow Region, Russian Federation*

Crystal structure and supramolecular organization of new segmented thermoplastic polyurethane ureas and their nanocomposites with ultra-small additives (less than 0.1 wt.%) of single-walled carbon nanotubes (SWCNTs) have been been investigated using DSC and X-ray diffraction analysis. Taking into account the Avrami model, effects of physical aging and thermal history of the samples on the crystallization rate was described. It was demonstrated that the introduction of ultra small amounts of SWCNTs does not decrease the crystallinity, but decreases the crystallization rate.

Key words: polyurethane, polyurethane urea, thermoplastic elastomer, single-walled carbon nanotubes, crystallization, phase separation, DSC, X-ray diffraction analysis.

Thermoplastic elastomers (TPEs) are block copolymers consisting of thermodynamically incompatible soft and rigid blocks, whose phase separation leads to the formation of nanodomains. Such a structure provides the opportunity to transform TPE-based materials into a viscous-fluid state at an elevated temperature using an environmentally friendly technology for molding and processing products. Among the existing types of TPEs, segmented thermoplastic polyurethanes and polyurethane ureas (TPUUs) are of great interest, and they have already become widely applied in industry due to their unique mechanical properties, durability, easy processing, *etc*.[1—5]

The rigid domains contain a large number of urethane or urethane urea units maintaining physical crosslinking through hydrogen bonds. The soft domains are hydroxy-containing polyesters capable of crystallizing at room temperature. In this case, the crystals play a role of additional nodes of the physical network, providing high strength characteristics to the material.[6]

On the one hand, TPUUs possess one among the highest values in terms of fabrication amounts, so improvements of their functional properties will expand the area of their application.[7—9] On the other hand, these polymers are an interesting example of the structure formation at various levels, thus being the excellent model system to explore the effect of morphology on macroscopic properties. First of all, this is related to a nontrivial nature of the mutual influence of two competing processes: the microphase separation of thermodynamically incompatible soft and rigid blocks and the crystallization of flexible TPUU moieties. Such processes occurring in many polymers and composites often determine the tendencies in the formation of their structure and in their physical and mechanical properties. In particular, the optimization of fraction of the crystalline phase as well as the size of crystallites in the domains of soft block allows mechanical properties of the material to be tuned for specific applications.

Obviously, the kinetics of crystallization depends on the both size of the domains and properties of the surrounding matrix. The phase-separated morphology sets the nature of crystallization of the soft block in nanodomains and imposes certain limitations on the degree of crystallinity, the size, and the shape of crystallites.[10—13] Depending on the toughness of amorphous block and the ratio between glass transition and melting temperatures of the soft block, there are two types of geometric constraints imposed on the crystallization process, the soft and hard confinements.[14,15] In the case of hard confinements, the

* Based on the materials of the XXI Mendeleev Congress on General and Applied Chemistry (September 9—13, 2019, St. Petersburg, Russia).

Published in Russian in *Izvestiya Akademii Nauk. Seriya Khimicheskaya,* No. 9, pp. 1740—1748, September, 2020.
1066-5285/20/6909-1

crystallization is limited by the size of soft block domains and does not break the main phase-separated morphology. If the driving force of phase separation is insufficient, the initial domain structure of block copolymer may be disturbed due to the "break-out" crystallization and reorganization of polymer morphology.[16—18]

Thus, the interaction between the processes of phase separation and crystallization of soft block causes a significant effect on the final structure of polymer and its mechanical properties.

The processes of phase separation and nucleation can be controlled *via* introducing nano-additives, the nucleating agents, whose examples include carbon nanofillers.[19—31] The nucleating effect arises due to the similar structures of filler and polymer matrix, which allows accelerating the kinetics crystallization. Investigations have revealed that some nanoadditives not only affect the crystallization kinetics of semi-crystalline polymers, but also improve the phase separation between their rigid and soft domains, thus affecting the mechanical properties.[32]

Thus, it has been found[33] that the enthalpy of crystallization and the degree of crystallinity of polyurethane nanocomposite based on poly(ε-caprolactone) in the presence of 2.5 wt.% multi-walled carbon nanotubes (CNTs) are higher than those of the initial sample. However, in another work,[34] there was observed a decrease in these parameters for a polyurethane composite based on the same components in the presence of multi-walled CNTs. Thus, the effect of CNTs on the crystallization kinetics depends on many factors. In general, we cannot assume whether CNTs are nucleating agent or topological defects for a particular type of the matrix.

We have earlier synthesized[35] a new multiblock polyurethane urea copolymer (TPUU) based on hydroxy-containing polyester poly(1,4-butylene glycol adipate) (PBA), two types of diisocyanates of aliphatic and aromatic nature, and chain extenders of various structures. The morphology of synthesized polymer was evaluated using X-ray diffraction (XRD) analysis and differential scanning calorimetry (DSC), and it was found during storage of the samples for several years that their crystal structure and mechanical properties were changing (*i.e.*, physical aging). We have explained this phenomenon by the continuous process of phase separation of blocks, which leads to an increase in the size of soft block domains and an improvement in the order in PBA crystals. It was found using small-angle X-ray scattering (SAXS) that TPUU immediately after molding possesses a nanodomain phase-separated structure, which is characteristic of block copolymers with the thermodynamically incompatible blocks. During the crystallization of soft block, a lamellar semi-crystalline morphology is formed. In this case, we expect keeping of the phaseseparated structure, *viz.*, a hard type of geometric confinement is observed. A fibrillar structure is formed upon stretching the samples after reaching the limit of forced high elasticity. Heating of the oriented films above the melting point of soft block crystals leads to a shrinkage of the material, while the phase-separated structure of block copolymer is preserved.

In the present work, the effects of physical aging and the presence of single-walled carbon nanotubes (SWCNTs) at low concentrations on the crystallization kinetics of multiblock polyurethane ureas were investigated using a combination of DSC and XRD methods in order to reveal the role of competing processes of the phase separation and recrystallization during the structure formation of these materials.

Experimental

SWCNTs were obtained according to the electric arc method using a Ni/Y catalyst, purified *via* oxidation in air to remove amorphous carbon, and treated with hydrochloric acid to remove metal particles until a content of the major product was at least 95%.[36] The diameter and length of SWCNTs were 1.4—1.6 nm and 2—10 μm, respectively. After the purification, the nanotubes were in the form of bundles (ropes) with a thickness from 50 to 150 nm. he specific surface of a nanotube powder, measured using nitrogen adsorption, was ~300 $m^2 g^{-1}$.

Samples of TPUUs were synthesized according to the known three-step method[35] from PBA (molecular weight of 2000 Da), a mixture of aliphatic 1,6-hexamethylene diisocyanate (HMDI) and aromatic 2,4-toluene diisocyanate (TDI), and also chain extenders: 1,4-butanediol (BD) and 2-amino-1-ethanol (EA). The reaction was carried out in dichloromethane solution in the presence of dibutyltin dilaurate (DBTDL) catalyst. To evaluate the crystallization of as-prepared TPUU during its aging, the samples were stored for two weeks (TPUM-0.5) and 60 months (TPUM-60) at 20 °C.

To prepare polyurethane urea nanocomposites, SWCNTs were preliminarily dispersed *via* ultrasonication using an Ultrasonic generator IL10-0.63 apparatus for 20 min, then introduced into the polymer matrix according to the in situ method at the step of macrodiisocyanate at the concentrations of 0.002 wt.% (TPUU-60/SWCNT-0.002), 0.004 wt.% (TPUU-60/SWCNT-0.004), and 0.008 wt.% (TPUU-60/SWCNT-0.008), and finally, a chain extender was added until the stoichiometric ratio between the isocyanate groups and hydroxy groups. After vigorous stirring for several minutes, the reaction mixture was poured into a Teflon mold and dried at 40 °C for one day until a constant weight. To evaluate the crystallization of nanocomposites, the samples were stored for 60 months at 20 °C.

The identification of TPUU and their composites with SWCNTs at the various concentrations as well as the presence or absence of side reactions was carried out using IR spectroscopy. The spectra were recorded on a Brucker Alpha FTIR spectrometer using a multiple attenuated total reflection (ATR) module under the following conditions: measurement range 4000—360 cm^{-1}, measurement step 2 cm^{-1}, and the number of scans per spectrum 56.

Molecular weight characteristics of the synthesized polymers were using by gel permeation chromatography (GPC) on a GPCV 2000 chromatograph (Waters) equipped with refractometric and viscometric detectors, and also a Heleos-II light scattering detec-

Table 1. Molecular weight parameters for TPUU and its nanocomposites with SWCNTs

Sample	M_n	M_w	PDI
TPUU-60	30200	81500	2.7
TPUU-60/SWCNT-0.004	31600	82000	2.6
TPUU-60/SWCNT-0.008	34500	83500	2.4

Designations: M_n is number a verage molecular weight; M_w is a weight verage molecular weight; PDI is polydispersity index (M_w/ M_n).

tor (Wayatt). A set of two "PLGel mixC 300"·7.6 mm columns was used, the eluent was THF, the elution rate was 1 mL min^{-1}, and the column temperature was 35 °C. The molecular weight characteristics of polymer and its nanocomposites with SWCNTs at various concentrations are given in Table 1. Analysis of the GPC results indicates the absence of any effect of small SWCNT additives on the molecular weight parameters of polyurethane urea composites.

The ultrasonic treatment of SWCNTs was carried out on an Ultrasonic Generator IL10-0.63 instrument (rod diameter of 0.15 mm, power of 472 W, and frequency of 23000 Hz).

Experiments on SAXS and wide-angle X-ray scattering (WAXS) were performed using a Xenocs diffractometer equipped with a GeniX3D generator (λ = 1.54 Å) emitting a beam of 300×300 μm in the size. Two-dimensional diffraction patterns were recorded using a Pilatus 300k detector. The detector was placed at distances of 17 and 150 cm from the sample for the WAXS and SAXS experiments, respectively. The exposure time was 5 min for the TPUU-60 sample and 15 min for the TPUU-0.5 sample. A modulus of the wave vector s ($s = 2\cdot\sin\Theta\cdot\lambda^{-1}$, where Θ is the Bragg angle) was calibrated using reflections of seven diffraction orders from silver behenate. To estimate kinetics of the crystallization, the film was heated in the heating stage up to 100—150 °C, and then quickly transferred to the measuring chamber of diffractometer. The obtained two-dimensional diffraction patterns were analyzed using a software package created in the Igor Pro environment (Wavemetrics Inc.).[37]

The degree of crystallinity of the samples $\chi_1(t)$ as a function of time (t) was calculated from XRD data according to the following equation:[38]

$$\chi_1(t) = \frac{\int (I_{tot}(s,t) - I_{am}(s,t))s^2 ds}{\int I_{tot}(s,t)s^2 ds}, \quad (1)$$

wherein $I_{tot}(s,t)$ is the one-dimensional scattering profile recorded at time t after the start of crystallization, $I_{am}(s,t) = k\cdot I_{tot}(s,0)$ is the scattering intensity from amorphous regions, proportional to the scattering intensity of the sample observed immediately after cooling from the melt and normalized to the total scattering intensity.

Kinetics of the isothermal crystallization of native TPUU and its nanocomposites was estimated using DSC on a DSC 30 Mettler Toledo calorimeter under isothermal conditions. A weighted sample (10 mg) was placed in an aluminum pan, heated up to a temperature above the melting point of soft block (up to 80 and 150 °C for TPUU-60 and TPUU-60-2 samples, respectively) at the rate of 10 °C min^{-1} under a nitrogen atmosphere, and kept for 2 min to erase a thermal history of the samples. The samples were then quickly cooled to the crystallization temperature (25 °C) and kept for 120 and 180 min, and they were heated again at the rate of 10 °C min^{-1} up to 80 °C in order to determine the temperature and enthalpy of melting of the soft block. The crystallization process was monitored visualizing the exothermic crystallization peak on a DSC curve in the heat flux—time coordinates. The interval between the heat flux measurements was 100 ms.

A change in the relative degree of crystallinity $c_2(t)$ *vs.* time (t) during the isothermal crystallization was determined from the ratio between the integral enthalpy of melting of the crystalline phase of sample and the enthalpy of melting corresponding to 100% degree of crystallinity of PBA according to the following equation:[39]

$$\chi_2(t) = \frac{\int_{T_0}^{T_B} (\frac{dH}{dT})dT}{\Delta H_f^\circ}, \quad (2)$$

wherein T_0 is the temperature of beginning of melting, $T_в$ is the temperature of end of melting, and the enthalpy of melting ΔH_f equal to 95 J g^{-1} was determined from DSC thermograms of oligodiol PBA and data on the degree of crystallinity acquired by the XRD method.

Results and Discussion

Structures of TPUU and its composites was characterized using IR spectroscopy (Fig. 1). The IR spectra of films of the synthesized samples do not contain any absorption bands corresponding to free OH groups (PBA, BD, and EA) and NCO groups (TDI and HMDI) at 3623 and 2270 cm^{-1}, respectively, while there are absorption bands characteristic of stretching vibrations of carbonyl and amide groups of the urethane moiety (C=O and C—NH) at 1727 and 3321, and 1530 cm^{-1}, respectively.

Bands corresponding to stretching vibrations of the NH-group of urethane moiety linked *via* a hydrogen bond to the carbonyl group are about 1530 and 3321 cm^{-1}. The presence of these bands indicates the formation of a network of hydrogen bonds between the NH and C=O groups in domains of the rigid block and/or with oxygen of the ester or ether group of the soft block. The absorption peaks at 1727, 1689, and 1600 cm^{-1} arise due to vibrations of the free and hydrogen-bonded C=O groups, and also the amide group (NH—C=O), respectively. The presence of free and hydrogen-bonded C=O groups indicates the phase separation in the cases of native polyurethane and its nanocomposite. A sharp peak at 1161 cm^{-1} is characteristic of asymmetric stretching vibrations of the C—O—C group of polyester, while a small peak at 1062 cm^{-1} belongs to the urethane group of polyurethane. Stretching vibrations at 2944 cm^{-1} are characteristic of the asymmetric CH_2 moieties of polyester and of the symmetric CH_2 group of diisocyanate.

At low concentrations of SWCNTs in the polymer matrix, there are almost no complexes formed with the

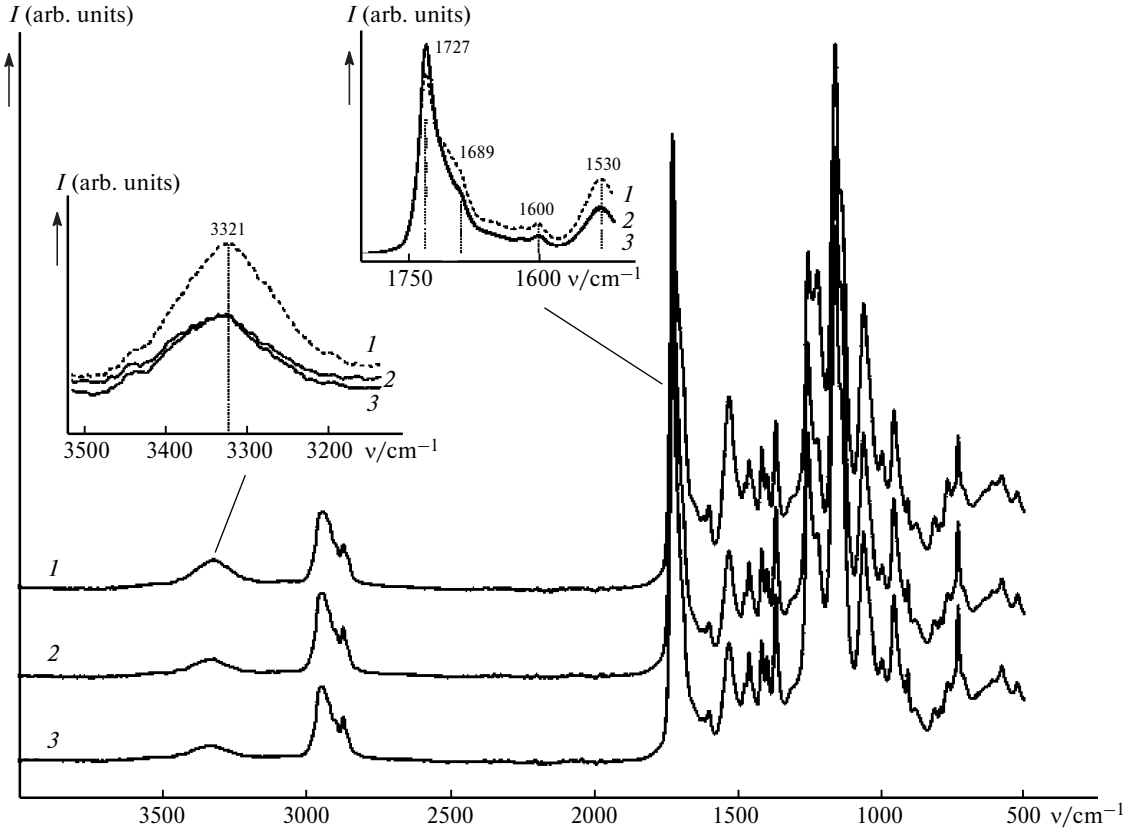

Fig. 1. IR spectra of the synthesized samples: TPUU-0.5 (*1*), TPUU-60/SWCNT-0.004 (*2*), and TPUU-60/SWCNT-0.008 (*3*). The insets show magnified areas for stretching vibrations of the N—H and C=O urethane groups.

amide and carbonyl groups of urethane, as evidenced by the absence of any shift in the absorption bands corresponding to the vibrations of these groups. At the same time, an increase in the intensity of bands of stretching vibrations of the free C=O groups at 1727 cm^{-1} and a decrease in the intensity of vibrations of the hydrogen-bonded C=O and N—H groups are observed at 1689, 3321, and 1530 cm^{-1}, respectively. It may be assumed that SWCNTs are located in the amorphous phase of TPUU, which causes the decreased density of network of the hydrogen bonds. This probably results in a change in the crystallization process of composite. Since the absorption band in the region of stretching vibrations of the C=O groups at 1727 cm^{-1} is a superposition of the absorption bands of urethane carbonyl groups and PBA ester bond, the degree of phase separation was not determined in the present work.

Figure 2 shows the DSC isotherms for TPUU samples with different storage period. The isotherm recorded at 25 °C for a TPUU-60 sample stored at room temperature for 60 months after its synthesis contains a characteristic endothermic peak (see Fig. 2, *a*) corresponding to the crystallization of soft block. An increase in the crystallization temperature up to 30 °C leads to a broadening of the peak. This phenomenon is characteristic of the classical dependence of crystallization rate on the temperature at low supercooling temperatures. The absence of any endothermic peak at 35 °C indicates an extremely low crystallization rate, which cannot be detected using the classical DSC method. There is another outcome for the sample stored for two weeks after its synthesis (TPUU-0.5) (see Fig. 2, *b*). A sharp peak is observed on the isotherm at 20 °C, while it noticeably broadens at 25 °C and disappears at 30 °C. Since there are no chemical transformations in the samples during their long-term storage,[32] it can be assumed that the differences in the crystallization kinetics are related to structural changes in the soft block domains during their long-term storage at room temperature.

Since the crystallization proceeds under hard geometric confinements, the structural differences observed in the phase-separated morphology may remain even after the melting of crystalline phase.

To confirm this assumption, the kinetics of sample crystallization at room temperature was investigated using SAXS and WAXS methods (Figs 3 and 4). Figure 3 shows the one-dimensional WAXS diffractograms that were recorded during the crystallization of TPUU samples differing in the storage time after their synthesis. A comparison of the one-dimensional diffraction patterns of initial TPUU-60 samples (see Fig. 3, *a*, curve *1*) and

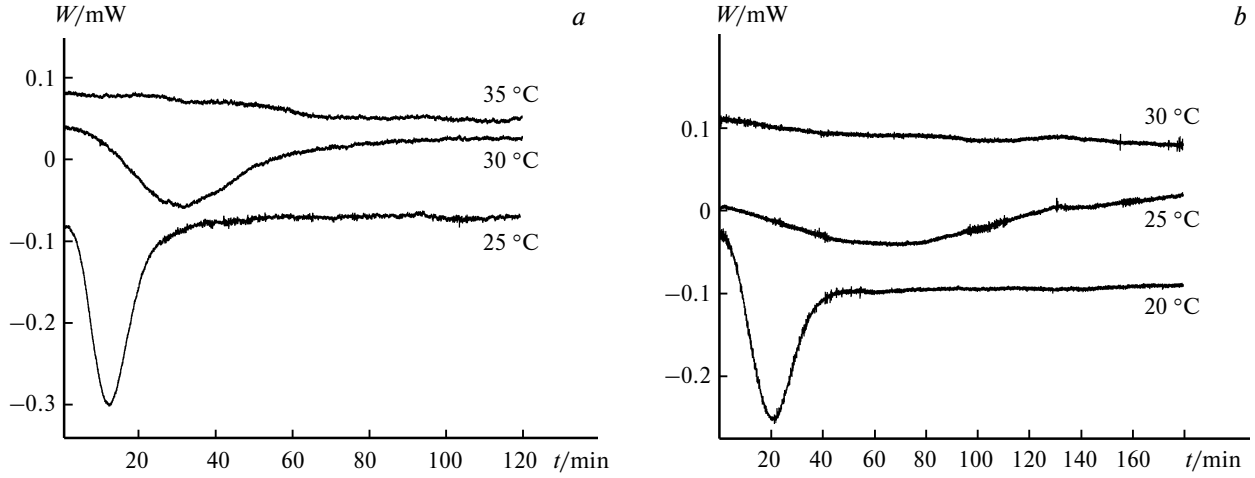

Fig. 2. Crystallization isotherms recorded at different temperatures for the TPUU-60 (*a*) and TPUU-0.5 (*b*) samples differing in their storage time (for clarity, the curves are shifted along the *Y* axis).

TPUU-0.5 (see Fig. 3, *b*, curve *1*) revealed significant differences in their crystal structure. The long-term storage leads to an increase in the degree of crystallinity (from 0.29 to 0.51)[32] and the increased size of PBA crystals, which is indicated by the increased intensity of narrow peaks corresponding to the crystalline structures and by a decrease in their half-widths (see Fig. 3, *a*, *b*, curve *1*, dashed line). Immediately after cooling the both samples from 70 to 25 °C, only a wide amorphous halo is observed for them on the one-dimensional profiles (see Fig. 3, *a*, *b*, curve *2*), indicating the complete melting of crystallites of the soft block. After 15 min from the beginning of crystallization, the diffractogram of TPUU-60 sample exhibits the appearance of narrow peaks (see Fig. 3, *a*, curve *3*) corresponding to the crystalline structures of PBA, while there are no any crystal peaks for TPUM-0.5 (see Fig. 3, *b*, curve *3*). This indicates that at 25 °C, the rates of nucleation and growth of the crystalline phase in the domains of soft block increase significantly after long-term storage of the samples. After 600 min of crystallization, there are

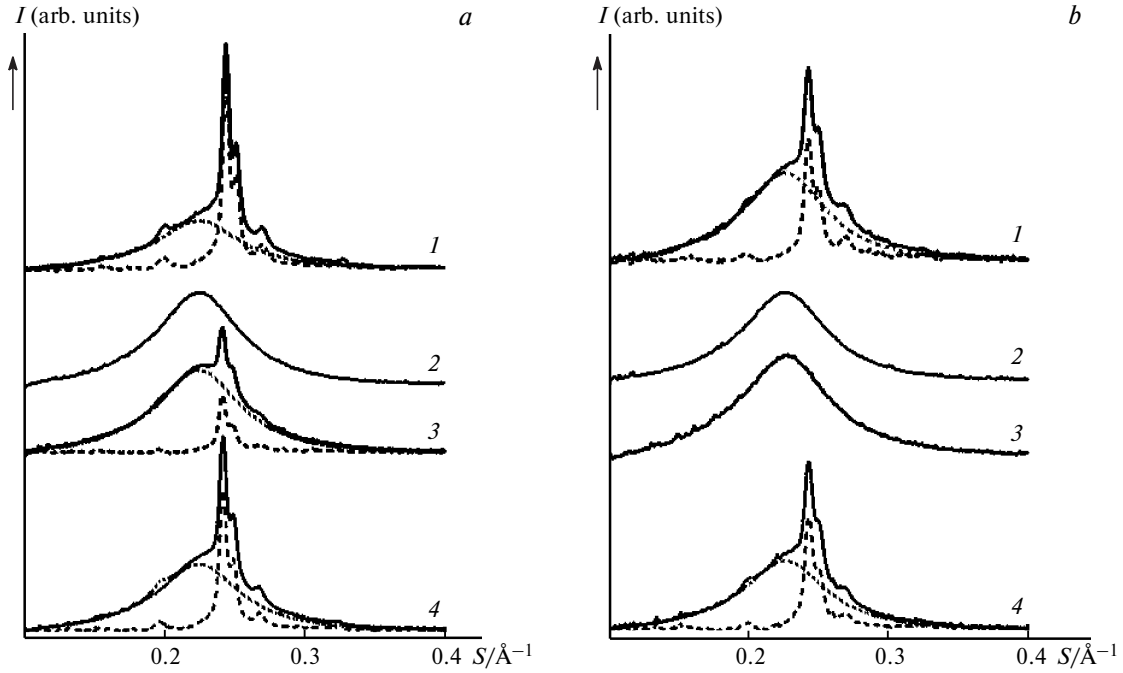

Fig. 3. WAXS diffraction patterns for the TPUM-60 (*a*) and TPUM-0.5 (*b*) samples: initial ones (*1*), immediately after their cooling down to room temperature (*2*), and 15 (*3*) and 600 min (*4*) after their cooling (dashed and dotted lines represent crystalline and amorphous components, respectively).

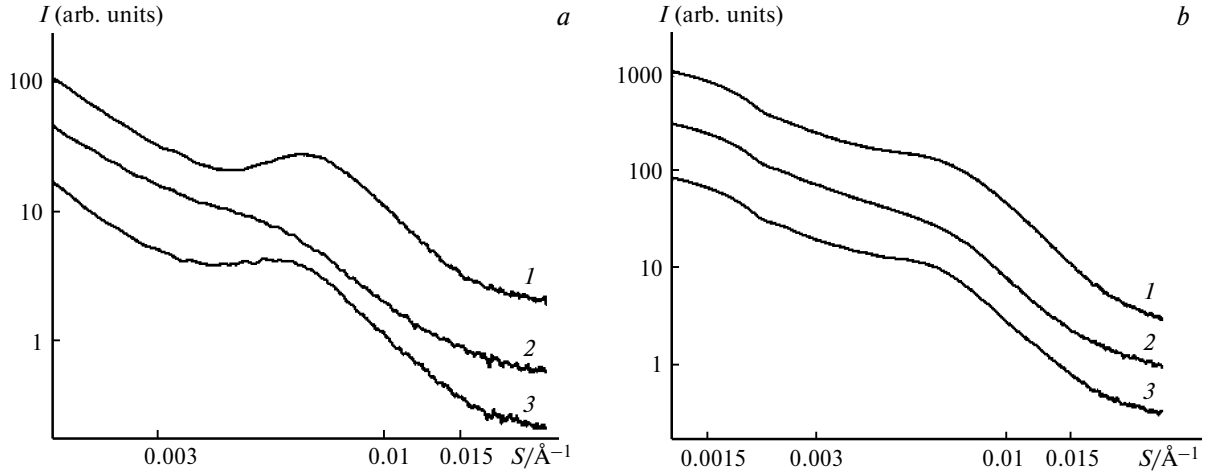

Fig. 4. One-dimensional scattering profiles of the SAXS diffraction patterns for the TPUM-60 (*a*) and TPUM-0.5 (*b*) samples: initial ones (*1*), 15 (*2*) and 600 min (*3*) after their cooling.

no more visible changes in the diffraction patterns, which indicates the completion of fast step of the crystal growth (see Fig. 3, *a*, *b*, curve *4*). However, it can be noted that the degree of crystallinity of the TPUM-60 sample at the end of crystallization is equal to 0.25 and close to that for the freshly prepared TPUM-0.5.

The process of physical aging also causes a strong effect on the morphology of samples. Figure 4, *a*, *b* shows the one-dimensional SAXS diffractograms for TPUU samples after their storage for different times. Diffraction patterns of the initial samples contain the maximum at 0.007 $Å^{-1}$, which indicates the formation of regular stacking of crystallites[35] (see Fig. 4, *a*, *b*, curve *1*). The scattering profiles recorded immediately after cooling the samples from 70 to 25 °C exhibit the presence of broad maximum in the region of 0.005 $Å^{-1}$ (see Fig. 4, *a*, *b*, curve *2*). Since the WAXS curves correspond to the amorphous state of samples (see Fig. 3, *a*, *b*, curve *2*), it was assumed that the phase-separated morphology was preserved in the samples during the melting of PBA crystallites. During the crystallization, this maximum is shifted to the region of large angles, while the scattering intensity decreases (see Fig. 4, *a*, *b*, curve *3*). Such a behavior is related to a change in the phase contrast between the soft and rigid blocks, as well as to the formation of ordered crystalline phase of the soft block. These processes are most clearly manifested for the TPUM-60 sample (see Fig. 4, *a*).

Analysis of the SAXS peak position revealed that the crystallization of soft block in a freshly prepared sample is completed within few hours, while that in the sample stored for 60 months takes less than 1 h. These data correlate with the results of changes in the degree of crystallinity acquired from the WAXS patterns (see Fig. 3, *b*). Therefore, the XRD results of samples storaged for different times revealed the difference in the crystallization rate at 25 °C and in the final semi-crystalline structure, which is due to the efficient process of phase separation during the long-term storage and to the formation of larger soft block domains. A complexity of the chemical structure of TPUU chain hinders a detailad describtion of the structure of crystalline phase of soft block. This aspect will be in depth explored later in our upcoming works, based on the analysis of model compounds.

The effect of phase separation processes on the crystallization kinetics in the isothermal mode was explored in more details according to the classical Avrami equation:[40]

$$1 - \chi(t) = \exp(-K_t t^n), \quad (3),$$

wherein $\chi(t)$ is the relative degree of crystallinity at the time t, exponential factor n is the constant so-called the Avrami exponent and depending on the mechanism of nucleation and the shape (geometry) of growing crystals, and parameter K_t is the rate constant including the rates of nucleation and crystal growth. To estimate the parameters n and K_t, the experimental dependence $\chi(t)$ is represented in double logarithmic coordinates:

$$\log(-\ln(1 - \chi(t)) = n\log t + \log K_t. \quad (4)$$

Using the values of n and K_t, one can calculate the half-time value ($t_{1/2}$) for the crystallization:

$$t_{1/2} = \left(\frac{\ln 2}{K}\right)^{1/n}. \quad (5)$$

Figure 5 shows the experimental time dependences for the degree of crystallinity of the TPUU-0.5 and TPUU-60 samples, which were extracted from the DSC isotherms at 25 °C and XRD data acquired at room temperature. As one can see, the curves possess a characteristic *S*-shaped form, and the degree of crystallinity for the TPUU-60 sample determined using the XRD method increases more slowly than that in the case of DSC experiment.

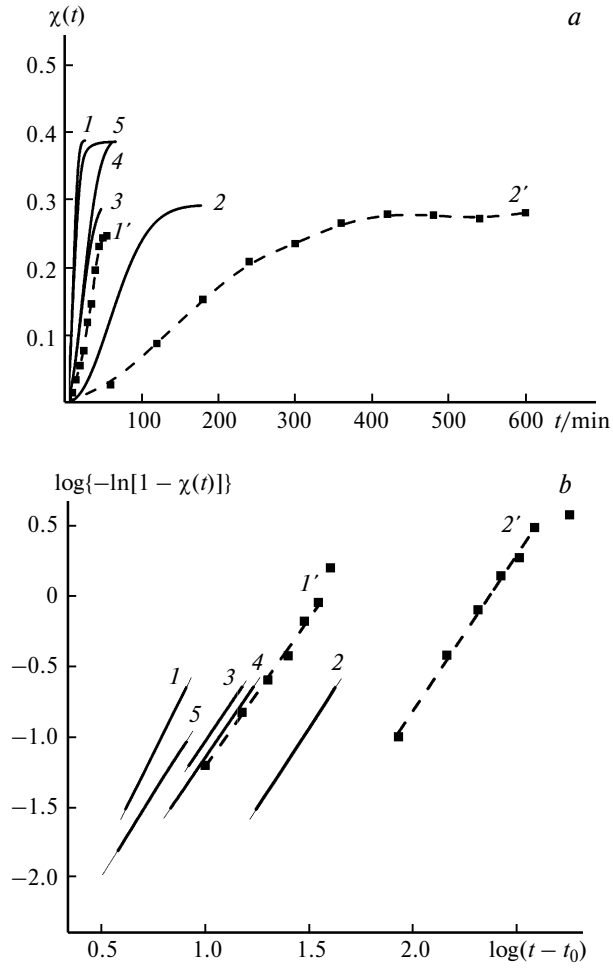

Fig. 5. (*a*) Dependences of the relative degree of crystallinity $\chi(t)$ on the time (t) during the aging process at room temperature, revealed using DSC (solid lines) and XRD (dashed lines) methods; (*b*) the same dependences plotted in the Avrami coordinates for the TPUU-60 (*1*, *1′*), TPUU-0.5 (*2*, *2′*), TPUU-60/SWCNT-0.004 (*3*), TPUU-60/SWCNT-0.008 (*4*), and TPUU-60-2 (*5*) samples.

This may be due to a better temperature control in the DSC cell.

The Avrami exponents (Tables 2 and 3) reflecting the mechanisms of nucleation and growth of the crystals were calculated from the dependences of degree of crystallinity on the time, acquired by XRD and DSC methods, using the approximation of linear region (Fig. 5, *b*). Figure 5, *b* shows the kinetic curves plotted in the Avrami coordinates, $\log\{-\ln[1-\chi(t)]\}$ *vs.* $\log(t-t_0)$; the regression coefficient is 1, which confirms the correctness of calculations, while the parameters n and K_t are determined in the region of $\chi(t)$ values from 5 to 25%.

According to the results calculated from the DSC curves, an increase in the parameters n_2 and K_{t2} is observed for the TPUU-60 sample stored for the long time. Such a behavior of the crystallization kinetics can be attributed to changes in the shape of nuclei, as well as in the nucleation mechanism itself due to the retention of phase-separated regions of the soft and rigid blocks. It may be assumed that the ordered regions of polyester units are preserved in the samples. Thus, the number of nuclei of the crystallization remains constant. The nature of nucleation is athermal. Due to the small volume of crystallizing region, there are no diffusion restrictions.

The Avrami parameters calculated from the XRD data for the TPUU-60 sample are noticeably different from the corresponding values revealed by the DSC method. This may be due to differences in the maximum heating temperature during the DSC and XRD investigations, 80 and 150 °C, respectively. It may be assumed that the soft blocks are completely isotropized at 150 °C, resulting in the decrease in the number of nuclei during the crystallization, which leads to a decrease in n. At this end, the crystallization kinetics depends on the efficiency of phase separation process, as well as on the thermal history of samples.

To estimate the influence of thermal prehistory of the samples on the processes of nucleation and growth of the crystals, experiments on isothermal crystallization of TPUU-60 were carried out after its heating up to 150 °C (TPUU-60-2) (see Fig. 5, *a*, *b*, curve *5*). A comparison of curves *1* and *5* plotted in Figure 5, *b* allows one to conclude that the crystallization process is accelerated upon an increase in the maximum heating temperature. This is apparently due to an increase in the mobility of polymer chains. The decrease of n from 2.96 to 2.34 may be caused by braking of the phase-separated morphology and the appearance of diffusion constrains due to the presence of

Table 2. Parameters of the crystallization kinetics for the initial TPUU and its nanocomposites at 25 °C (revealed using DSC)

Sample	T_m/°C	ΔH_f/J·g^{-1}	$\chi_2(t)$	n_2	$K_{t2}\cdot10^{-4}$/min^{-n}	$t_{1/2}$/min
TPUU-0.5	52.0	28.0	0.28	2.27	0.46	69.0
TPUU-60	55.7	48.9	0.36	2.96	4.55	12.0
ТПУМ-60-2	58.7	44.5	0.38	2.34	10.1	13.4
TPUU-60/SWCNT-0.004	55.9	46.7	0.38	2.19	6.03	25.5
TPUU-60/SWCNT-0.008	55.6	45.0	0.38	2.17	4.87	28.2

Note: ΔH_f is the enthalpy of melting upon the first heating, and $\chi(t)$ is the relative degree of crystallinity vs. time t during the crystallization.

Table 3. Parameters of the crystallization kinetics for the initial TPUU, revealed using the XRD analysis

Sample	$\chi_1(t)$	n_1	$K_{t1} \cdot 10^{-4}/\text{min}^{-n}$
TPUU-0.5	0.25	2.21	0.05
TPUU-60	0.28	2.39	2.14

polyurethane moieties close to the crystallization front. In this case, the degree of crystallinity and the melting point of crystalline phase do not depend on the maximum heating temperature (see Table 2).

Therefore, the processes of phase separation of the rigid and soft blocks during the physical aging cause a serious effect on the kinetics of formation of the additional physical network in the TPUU samples due to the PBA crystallization.

Another approach to control the diffusion factor affecting the structure and properties of thermoplastic elastomers is the introduction of nanofillers, in particular SWCNTs,[41,42] into the polymer matrix. In the present work, the crystallization kinetics of polyurethane composites with SWCNTs at their different concentrations was competitively evaluated along with the native TPUU at 25 °C upon storage for 90 min immediately after their cooling (see Fig. 5). Such a selection of the temperature is due to the efficient proceeding of crystallization of native TPUU under these conditions.

The *S*-shaped dependences of degree of crystallinity on the time (see Fig. 5, curves *3* and *4*) were plotted using the crystallization isotherms of composites at 25 °C, recorded in the DSC measurements.

As one can see from Table 2, the introduction of SWCNTs causes no effect on the melting point of PBA crystallites and on the final degree of crystallinity. However, the presence of nanotubes (0.004 and 0.008 wt.%) leads to the decreased crystallization rate of soft block and to a decrease in the value of n_2 from 2.9 to 2.2, while parameter K_{t2}, on the contrary, increases. This observation is apparently related to a change in the growth mechanism of crystalline lamella and to the transition from the athermal nucleation, characteristic of native TPUU, to a mixed nucleation due to the presence of SWCNTs. In addition, the SWCNT filler plays the role of diffusion constrain during the lamellae growth. This assumption is consistent with the data reported previously in other works.[28—30] It should also be noted that the introduction of SWCNTs increases the half-time value ($t_{1/2}$) for the transformation. It may be assumed that SWCNTs are not the nucleation centers, but act as objects that physically hinder the diffusion of PBA macromolecular moieties and consequently reduce the mobility of polymer chains in a close proximity to the crystal growth front. A similar phenomenon has earlier been observed upon the introduction of multiwalled CNTs (1—5 wt.%) into a polyurethane matrix.[33]

In summary, the present work reports on the DSC and XRD investigations of the fast crystallization processes and the slow processes of phase separation of the starting TPUU samples during their aging at room temperature, as well as of their nanocomposites with SWCNTs loaded at low concentrations (0.002—0.008 wt.%), as the dependences on the crystallization conditions and thermal prehistory of samples. The analysis of experimental data revealed that the slow processes of phase separation of the soft and rigid blocks occur in the samples upon their long-term storage for 60 months. The increase in the size of domains of the soft block was confirmed by the drustical increase in the rate of isothermal recrystallization from the melt, as compared to the fresh samples. This effect is probably related to increases in the nucleation rate due to the presence of partial chain ordering and in the size of the soft block domains. It should be noted that the increase in the size of crystallizing domains in the samples after their long-term storage does not lead to a noticeable increase in the degree of crystallinity after the isothermal recrystallization.

Based on the analysis of the thermodynamic parameters and the degree of crystallinity, it was found that the presence of SWCNTs does not cause changes in the morphology, but slows down the crystallization rate. A decrease in the Avrami exponent (n) and an increase in the value of K_t upon increasing the filler concentration are related to the transition from the athermal nucleation to the mixed one. Therefore, the introduction of small amounts of the SWCNTs into the polymer matrix allows one to control the diffusion factor and to tune the rate of composite crystallization.

This work was financially supported by the Russian Foundation for Basic Research (Project No. 19-53-15016) and carried out within the framework of the state task No. 0089-2019-0012 (Registration No. AAA-A19-119032690060-9).

References

1. M. F. Schulz, F. S. Bates, K. Almdal, K. Mortensen, *Phys. Rev. Lett.*, 1994, **73**, 86.
2. I. W. Hamley, *Adv. Polym. Sci.*, 1999, **148**, 113.
3. Y. L. Loo, R. A. Register, *Crystallization within Block Copolymer Mesophases, In Development in Block Copolymer Science and Technology*, Wiley, New York, 2004, 367 p.
4. A. J. Muller, V. Balsamo, M. L. Arnal, *Polym. Sci.*, 2005, **190**, 1.
5. B. Nandan, J. Y. Hsu, H. L. Chen, *J. Macromol. Sci., Polym. Rev.*, 2006, **46**, 143.
6. R. E. Cohen, A. Bellare, M. A. Drzewinski, *Macromolecules*, 1994, **27**, 2321.
7. D. J. Quiram, R. A. Register, G. R. Marchand, A. J. Ryan, *Macromolecules*, 1997, **30**, 8338.
8. J. T. Xu, S. C. Turner, J. P. A. Fairclough, S. M. Mai, A. J. Ryan, *Macromolecules*, 2002, **35**, 3614.

9. V. P. Grachev, A. S. Dzhalmukhanova, E. A. Yurieva, S. A. Kurochkin, V. A. Barachevsky, A. M. Gorelik, N. L. Zaichenko, S. M. Aldoshin, *Russ. Chem. Bull.*, 2018, **67**, 535.
10. L. Zhu, S. Z. D. Cheng, B. H. Calhoun, Q. Ge., R. P. Quirk, E. L. Thomas, B. S. Hsiao, F. Yeh, B. Lotz, *J. Am. Chem. Soc*., 2000, **122**, 5957.
11. L. Zhu, B. R. Mimnaugh, Q. Ge, R. P. Quirk, S. Z. Cheng, E. L. Thomas, B. Lotz, B. S. Hsiao, F. Yeh, L. Liu, *Polymer*, 2001, **42**, 9121.
12. Y. Sen Sun, T. M. Chung, Y. J. Li, R. M. Ho, B. T. Ko, U. S. Jeng, B. Lotz, *Macromolecules*, 2006, **39**, 5782.
13. H.-L. Chen, C.-J. Wu, T.-L. Lin, J. S. Lin, *Macromolecules*, 2001, **34**, 6936.
14. Y. Zhou, S. K. Ahn, R. K. Lakhman, M. Gopinadhan, C. O. Osuji, R. M. Kasi, *Macromolecules*, 2011, **44**, 3924.
15. B. Nandan, J. Hsu, H. Chen, *J. Macromol. Sci*., *C*, *Polym. Rev.*, 2006, **46**, 143.
16. S. Y. Yu-Su, S. S. Sheiko, H. L. Lee, W. Jakubowski, A. Nese, K. Matyjaszewski, D. Anokhin, D. Ivanov, *Macromolecules*, 2009, **42**, 9008.
17. J. T. Xu, J. P. Fairclough, S. M. Mai, A. J. Ryan, C. Chaibundit, *Macromolecules*, 2002, **35**, 6937.
18. Y. L. Loo, R. Register, A. J. Ryan, *Macromolecules*, 2002, **35**, 2365.
19. B. A. Fathilah, M. Raja, *Polym. Comp.*, 2010, **31**, 1309.
20. R. T. Zeng, W. Hu, M. Wang, S. D. Zhang, J. B. Zeng, *Polym. Test*., 2016, **50**, 182.
21. T. Yaricia, M. Kodal, G. Ozkoc, *Polymer*, 2018, **146**, 361.
22. D. G. Papageorgiou, Z. Terzopoulou D. S. Achilias, D. N. Bikiaris, M. Kapnisti, D. Gournis, *Polymer*, 2013, **54**, 4604.
23. G. Z. Papageorgiou, D. S. Achilias, S. Nanaki, T. Beslikas, D. Bikiaris, *Thermochim. Acta*, 2010, **511**, 129.
24. J. Schawe, P. Pötschke, I. Alig, *Polymer*, 2017, **116**, 160.
25. S. R. Vaaben, A. Aguilar, F. Avalos, L. F. Ramos-de Valle, *J. Therm. Anal. Calorim.*, 2008, **93**, 947.
26. J. Li, Z. Fang, L. Tong, A. Gu, F. Liu, *Eur. Polym. J.*, 2006, **42**, 3230.
27. C. A. Mitchell, R. Krishnamoorti, *Polymer*, 2005, **46**, 8796.
28. H. Zeng, C. Gao, Y. Wang, P. C. P. Watts, H. Kong, X. Cui, D. Yan, *Polymer*, 2006, **47**, 113.
29. B. P. Grady, F. Pompeo, R. L. Shambaugh, D. E. Resasco, *J. Phys. Chem. B*, 2002, **106**, 5852.
30. V. V. Arslanov, M. A. Kalinina, E. V. Ermakova, O. A. Raitman, Yu. G. Gorbunova, O. E. Aksyutin, A. G. Ishkov, V. A. Grachev, A. Yu. Tsivadze, *Russ. Chem. Rev.*, 2019, **88**, 775.
31. A. L. Didenko, V. E. Smirnova, E. N. Popova, G. V. Vaganov, D. A. Kuznetsov, V. M. Svetlichny, O. V. Tolochko, E. S. Vasilieva, V. E. Yudin, V. V. Kudryavtsev, *Russ. Chem. Bull.*, 2019, **68**, 1603.
32 J. Z. Xu, G. J. Zhong, B. S. Hsiao, *Prog. Polym. Sci.*, 2014, **39**, 555.
33. N. G. Sahoo, Y. C. Jung, H. J. Yoo, J. W. Cho, *Compos. Sci. Technol.*, 2007, **67**, 1920.
34. R. N. Jana, J. W. Cho, *Compos. A*, 2010, **41**, 1524.
35. D. V. Anokhin, M. A. Gorbunova, Ya. I. Estrin, V. V. Komratovaa, E. R. Badamshina, *Phys. Chem. Chem. Phys.*, 2016, **18**, 31769.
36. A. V. Krestinin, *Mendeleev Chemistry Journal* [*Zhurn. Ross. Khim. Ob-va im. D. I. Mendeleeva*], 2004, **43**, 21 (in Russian).
37. R. J. May, C. Gentilini, D. E. Clarke, Ya. I. Odarchenko, D. V. Anokhin, D. A. Ivanov, K. Feldman, P. Smith, M. M. Stevens, *RSC Adv.*, 2014, **4**, 2096 L.
38. L. E. Alexander, in *X-ray Diffraction Methods in Polymer Science*, Wiley-Interscience, New York, 1969, 137.
39. B. Wunderlich, in *Thermal Analysis*, Academic Press, 1990, 417.
40. M. J. Avrami, *Chem. Phys.,* 1939, **7**, 1103.
41. F. L. Q. Ferreira, M. C. Lopes, A. P. M. Lopes, R. L. Lavall, G. G. Silva, *Polím.: Ciênc. Tecnol.*, 2019, **29**, e2019012.
42. M. Kuběna, M. Eliáš, L. Zajíčková, J. Poduška, T. Kruml, *Adv. Mater. Sci. Eng.*, 2019, Article ID 6598452, 8.

Received October 2, 2019;
in revised form February 27, 2020;
accepted June 10, 2020